PCCP

Accepted Manuscript

ROYAL SOCIETY OF CHEMISTRY

www.rsc.org/pccp

Network formation in graphene oxide composites with surface grafted poly-N-isopropyl amide chains in aqueous solution characterized by rheological experiments

Amin GhavamiNejad[a], Saud Hashmi[a,c], Han-Ik Joh[b], Sungho Lee[b], Youn-Sik Lee[a], Mohammad Vatankhah-Varnoosfaderani[a] and Florian J. Stadler*[a]

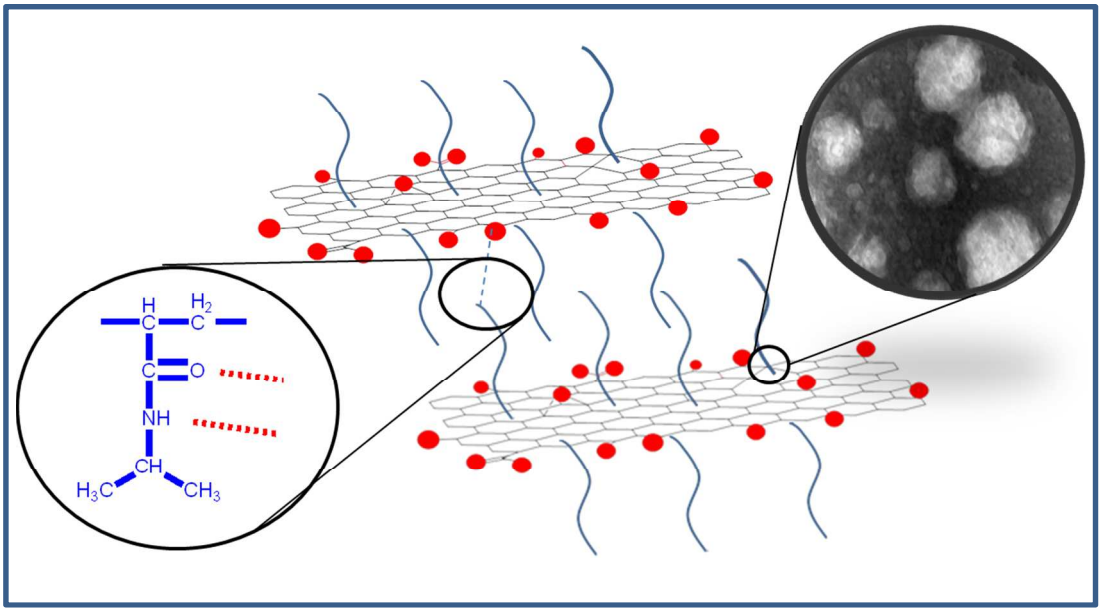

Cite this: DOI: 10.1039/c0xx00000x

www.rsc.org/xxxxxx

ARTICLE TYPE

Network formation in graphene oxide composites with surface grafted poly-N-isopropyl amide chains in aqueous solution characterized by rheological experiments

Amin GhavamiNejad[a], Saud Hashmi[a,c], Han-Ik Joh[b], Sungho Lee[b], Youn-Sik Lee[a] Mohammad Vatankhah-Varnoosfaderani[a,d]* and Florian J. Stadler[a]*

Received (in XXX, XXX) Xth XXXXXXXXX 20XX, Accepted Xth XXXXXXXXX 20XX
DOI: 10.1039/b000000x

Poly N-isopropyl acrylamide (PNI) radically polymerized in aqueous solution in the presence of graphene oxide (GO) can significantly change the properties of the resulting solution from a regular polymer solution to a soft solid with a GO content of only 0.176 wt.% (3 wt.% with respect to PNI). However, these properties require the presence of both grafting and supramolecular interactions between polymer chains and hydrophilic groups on GO (-OH, -COOH)., proven by Fourier transform infrared spectroscopy (FTIR), transmission electron microscopy (TEM), X-ray diffraction and spectroscopy (XRD) and Raman spectra. While very low GO-contents (below 0.05 wt.%) only lead to a labile structure, which can be disassembled by shear, higher contents yield composites with solid-like characteristics. This is clearly evident from the rheological behaviour, which changes significantly at a GO content around 0.15 wt.%. Intensive shearing destroys the weak network, which cannot reform quickly at lower GO-concentrations, while at intermediate concentrations, restructuring is fast. GO-contents of 0.176 wt.% lead to a material behaviour, which almost perfectly recovers from small deformations (creep and creep recovery compliance almost match) but larger deformations lead to permanent damage to the sample.

Introduction

Since its discovery in 2004, graphene has been extensively studied due to its attractive electronic, catalytic, mechanical, optical, and magnetic properties with great potential in various applications ranging from energy storage to biomedical materials.[1-3] The chemical structure of graphene oxide (GO) is heterogeneous and the coverage of oxygen groups varies depending on the degree of oxidation (primarily hydroxyl and epoxy groups) in the preparation processes.[1, 2] Unlike graphene, GO is hydrophilic, has abundant oxygen-containing functional groups, and can be excellently dispersed in different solvents including water.[3] As the basal plane of GO is much more hydrophobic than the carboxyl-decorated edges, the differences in both the hydrophilicity and structural dimensions make GO behave like an amphiphile.[4-7] The oxygen-containing functional groups on the basal plane and sheet edges allow GO to react with organic and inorganic chemicals so that a variety of functional hybrids and soft materials have been synthesized.[1, 8] The unique 2D structure, aqueous dispersability, immobilized carboxyl and hydroxyl surface defects, and residual C=C bonds have prompted researchers to anchor polymers and nanoparticles on GO surfaces using "graft onto'' and ''graft from'' strategies.[9-13] Based on these strategies, functional "soft" materials can be synthesized in a variety of forms including colloids, liquid crystals, gels, amphiphiles, membranes, foams, and polymeric materials.[14] Although soft materials or complex structured fluids[15] may not be strong and durable, their distinctive susceptibility and responsiveness to external stimuli are crucial for many applications ranging from sensors, cosmetics, and electronics to biomimetic applications.[16, 17] The characteristics are tailored by covalent and or supramolecular interactions among the functional groups, type and amount of solid fillers as well as the effect of external stimuli including temperature, pH, and shear forces.[18, 19]

In recent years, stimuli-responsive polymers have been grafted onto GO surfaces to produce multi-responsive, cost effective, and structurally defined soft materials with improved physical properties.[8, 20] Recently, several attempts have been made to harness the grafting of PNI on the surfaces of graphene and graphene oxide sheets.[21-23] For example, Qi *et al.*[23] prepared PNI-GO hybrids via *in situ* free-radical polymerization and they demonstrated reversible switching of its wettability upon exposure to near infrared light. Very recently, Dong *et al.*[24] demonstrated the possibility to graft a large amount of PNI-molecules and, thus, to immobilize them on the high surface area of graphene. Although several studies have been devoted to these hybrids and various practical applications have been demonstrated, there is a clear lack of understanding of the structure-property relationships concerning the behaviour of poly(N-isopropyl acrylamide) (PNI) on a two-dimensional (2D) surface.

In general, the type of polymer plays a vital role in improving the characteristic property relationships when grafting hydrophilic

polymers like chitosan, proteins, and bio-compactable polymers.[25-29] PNI can be grafted onto the surface or the edges of GO through covalent chemistry.[23] Due to its sensitivity to external stimuli, biocompatibility, hydrophilicity, and non-toxicity, water stable and biocompatible functional materials can be prepared. The prospect of their applications requires facile studies of these multi-phase complex fluids under different physiological conditions.

A notable observation is the qualitative resemblance between the thermo-mechanical responses of polymer nanocomposites and polymer thin films confined between planar surfaces.[25, 30] This similarity implies that the grafting of polymer chains on the surface of GO alters the chain mobility far into the bulk and, therefore, the mixture cannot be simply envisioned as a dispersion of hard particles interacting in a matrix but as a hard particle composite with an influence layer of polymer chains around it. Such composites generally exhibit strong nonlinear viscoelastic behaviour in response to dynamic inputs. Typical examples of such nonlinear characteristics are strong shear thinning at relatively low shear rates or strain-dependent viscoelastic moduli at low strain amplitudes.[31] The rheological behaviour of these nonlinear complex fluids is very complicated in terms of both processing and applications.[32-34]

The aim of this study was to determine the influence of the GO concentration on the behaviour of *in situ* polymerized PNI-GO composites. The results were compared to PNI-RGO (reduced graphene oxide) prepared under the same conditions as well as blends of PNI and GO.

Experimental

Materials

N,N,N',N'-tetramethylethylenediamine (TMEDA, Fluka, >99%) and ammonium peroxodisulfate (APS, Aldrich, >98%) were used as received. NIPAM (98% Aldrich) was recrystallized from a 65:35 (v/v) mixture of hexane:benzene before use. All aqueous solutions were prepared using ultrapure water purified with a Milli-Q UV-Plus water purification system. The preparation of GO and RGO is described in the SI.

Synthesis of PNIPAM-GO composites

According to previous reports of attaching PNI on graphene oxide,[23] PNI–GO nanocomposites were prepared via *in situ* free-radical polymerization. PNIPAM-GO nanocomposite suspensions were prepared as follows. GO was dissolved in 10 mL of water and sonicated for 120 min to make a homogenous brown dispersion (0.5 mg/mL). The NIPAM monomer was dissolved in distilled water and the GO aqueous dispersion was gradually added to the NIPAM solution to obtain homogeneous NIPAM-GO solutions by stirring under a N_2 atmosphere. The aqueous solution was also bubbled for 30 min with nitrogen gas to remove the dissolved oxygen in the solution. Next APS, and TMEDA (10 µmol/µL) in H_2O were added to the solution at 10°C under stirring. Then, free-radical polymerization was allowed to proceed for 24 h. The as-prepared PNI-GO suspension was homogeneous without precipitates and colourless to brown, depending on the GO content. Additionally, a PNI-RGO composite with an RGO content of 3 wt% with respect to the PNI content was also produced through the same procedure to compare the influence of the concentration of functional groups on the filler surface and to determine the effect of supramolecular interactions of PNI on the GO sheets the PNI+GO3 blend sample was produced by mixing the 500 mg PNI sample with 15 mg of GO.

It should be noted that the samples analysed by FTIR and TEM measurements were purified by repeated washing, dialysis, and centrifugation to remove free PNI. For the sample PNI M_w=3.2 10^6 g/mol and M_w/M_n=5.3 it was measured, which is discussed along with other materials elsewhere.[35] For the other materials in this study, it is impossible to determine a molar mass, as the polymers are partially polymerized on the surface of the GO- or RGO-sheets, leading to an unknown elution behaviour and potentially to significant damage to the GPC-setup.

Table 1: Composition of the PNI-GO-composites

Sample	Graphene Oxide [wt.%][a]	Graphene Oxide [mg]	Filler concentration [wt.% of total sample]
PNI-GO0.25	0.25	1.25	0.015
PNI-GO0.5	0.5	2.5	0.029
PNI-GO1	1	5	0.059
PNI-GO2	2	10	0.118
PNI-GO3	3	15	0.176
PNI-RGO3 [b]	3	15	0.176
PNI+GO3 [c]	3	15	0.176

[a] with respect to PNI.

[b] In this sample RGO as filler has been used.

[c] this sample was blended physically using PNI and GO.

In all cases, 8 cc of milli-Q water, 500 mg of NIPAM and 10 µL of initiator and accelerator were used, yielding a total of 6.25% (w/v) or 5.88 wt.% PNI. (Solution concentrations of initiator used is 1 mmol/mL water)

Characterization Techniques

FTIR

Fourier transform infrared spectroscopy (FTIR, Perkin-Elmer Spectrum One, USA) was employed to study the functionalization. GO, PNI-GO, and PNI dried powder were moulded into discs using KBr. It should be noted that the composites were washed several times by dialysis and centrifugation prior to the FT-IR measurements to remove any PNI not connected to the GO sheets.

XRD

X-ray diffraction experiments were performed at room temperature to study the crystalline structure of materials using an X-ray diffraction system (Philips X'Pert-MRD, the Netherlands) employing CuK_α radiation (X-ray wavelength λ = 1.5406 Å) under normal laboratory conditions. The chemical compositions and crystallographic structures of GO, PNI-GO, and PNI were recorded by varying the angle following Bragg's law, which is satisfied by the d-spacing in polycrystalline materials. Plotting the angular positions and intensities of the resultant diffracted peaks of the radiation produces a pattern which is characteristic of the sample, where a mixture of different phases are present.

Raman

Micro-Raman spectroscope (Nanofinder 30) with argon ion laser at the excitation wavelength of 632.8 nm, infrared spectroscope (Tokyo Instrument, INC)

TGA

Thermogravimetric analysis (TGA) measurements were run on a

SDT Q600 TGA/DSC system under a N2 purge from room temperature to 800°C at a heating rate of 10°C min^{-1}.

TEM

A Transmission Electron Microscope (TEM, JEOL(Japan)/ JEM-2010 operated at 200 KV) was used to demonstrate the morphology and 2D structural information of the GO and PNI-GO nanocomposites.

Rheology

The mechanical properties of the complex polymeric system were tested using a rheometer (Malvern KinexusPro) with a 50 or 20 mm/1° or 2° cone/plate geometry. A solvent trap with a liquid seal around the moving part of the geometry and an additional water reservoir was used to ensure a water saturated environment. By default, three test setups were used. The temperature dependence and lower critical solution temperature (LCST), in particular, were assessed by a temperature ramp with a heating rate of q=2°C/min from 5-80°C. An angular frequency of ω=0.16 s^{-1} and a deformation, γ_0, of about 30% in the linear viscoelastic regime were applied. The viscosity function was determined at T=25°C by a stress ramp test at a stress of σ=20 Pa. To avoid the effects related to sample ejection, the maximum shear rate was limited to $\dot{\gamma}$=4,000 s^{-1}. A strain sweep was performed at T= 25°C and ω=10 s^{-1} by increasing the shear from γ_0 = 0.01% to γ_0^{max}= 1000% in order to determine the mechanical stability of the samples at a high shear. The test was performed after the viscosity function, which served as means to reset the structure and, thus, get data with the same pre-treatment for all samples. Additionally, the test was repeated to ensure the absence of sample ejection and to check for the development of shear-induced structures which can occur if stable shear bands or stream-lined supramolecular structures develop.

Additionally, creep and creep recovery tests were performed by applying a constant shear stress, τ, to the specimen where the deformation, γ, was measured as a function of the creep time, t. The time dependent creep compliance, J(t), was determined as follows.

$$J(t) = \gamma/\tau \quad (1)$$

In a creep recovery test, the stress, τ, was set to zero at the creep time $t=t_0$ and the recoverable part of the deformation, γ_r, was recorded as a function of the recovery time, t_r, while it was set to 0 at $t_r=t_0$. γ_r is defined as follows.

$$\gamma_r(t_r,t_0)=\gamma(t_0)-\gamma(t_r + t_0). \quad (2)$$

The recoverable compliance is obtained from the recoverable part of the shear deformation $\gamma_r(t_r,t_0)$ as follows.

$$J_r(t_r,t_0) = \gamma_r(t_r,t_0)/\tau \quad (3)$$

Results

FT-IR and X-ray diffraction

Figure 1 shows a comparison of the absorption bands of GO, PNI and the PNI-GO composite. The spectrum of GO sheets shows a broad absorption band at 3410 cm-1 that is related to the OH groups, and an absorption band at 1635 cm-1 from the carbonyl groups of GO. It also showed bands due to epoxy (1200 cm-1) and alkoxy (1100 cm-1) groups situated at the edges of the GO nanosheets.[36, 37] In the spectrum of dry PNI, the absorption peak at 3280 cm-1 corresponds to the N-H bonds and absorption peaks at 2977–2890 cm-1 and 1631 cm-1 correspond to the C-H stretch and C=O stretch, respectively.[37] In the FTIR spectrum of the PNI-GO hybrids the strong peak of the C=O stretching vibration resulted from PNI and the peak at 3200 cm-1 assigned to the stretching vibration of N–H can be observed, which proves the existence of PNI on the surface of graphene oxide.[23, 24]

XRD was used to determine the degree of exfoliation of GO.[38] Figure 2 shows the XRD patterns of pure GO, pure PNI, and PNI-GO. The characteristic XRD peak of the pure GO sheets appeared at 2θ=11.26°, corresponding to an inter-planar spacing of 7.85 Å, which is significantly larger than the literature value of 3.35 Å reported for graphite.[39, 40] PNI showed a diffraction peak at 2θ=19.70°, which corresponds to the amorphous phase of the polymer. However, for the PNI-GO nanocomposite, its XRD pattern only shows the PNI diffraction peak from PNI and the diffraction peak of GO disappears. This clearly demonstrates the disappearance of the regular and periodic structure of the graphene sheets, the formation of fully exfoliated structures, and the homogeneous distribution of GO sheets in the polymer matrix.[36]

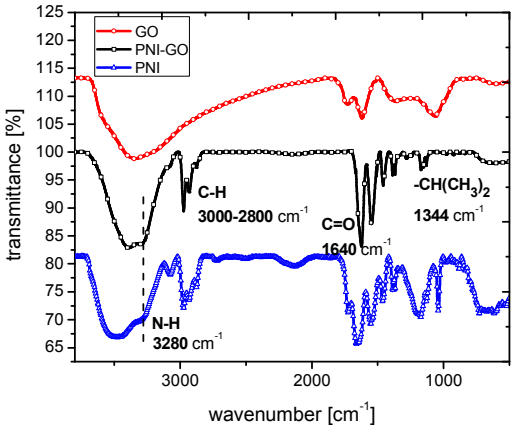

Figure 1: FT-IR data of GO, PNI-GO3 and PNI.

In other words as this peak in GO is about 3° wide, it can be concluded that galley-spacing peak of the composite, if it still exists, must be at 2θ ≤ 7°, which corresponds to d=12.6 Å. Considering that d=7.85° for GO is already considered to be highly distorted, it has to be concluded that PNI-GO3 contains GO, which has lost most, if not all, of its galley structure. In addition, it is also clear that the diffraction peak position between polymer and composite is slightly changed and has become asymmetric suggesting significant fraction of PNI with more free volume, which is attributed to proximity to the GO-sheets, where steric hindrance and surface interactions prevent closer average distances.

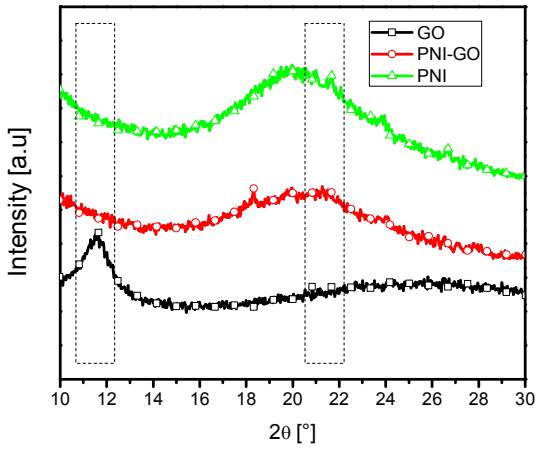

Figure 2: XRD data of GO; PNI–GO3, and PNI

Raman spectroscopy

Raman scattering is highly sensitive to the electronic structure of samples, and its result is often taken as evidence for the chemical functionalization of graphene sheets. The Raman spectrum of GO shows diamondoid D-band (defects/disorder-induced mode) assigned to the vibration of sp_2-hybridized carbon atoms at 1350 cm^{-1} and graphitic G-band (in-plane stretching tangential mode) assigned to the vibration of carbon atoms with dangling bonds in plane terminations of disordered graphite, indicating the formation of sp_3 carbons in GO at 1596 cm^{-1}, with an almost equal intensity of diamondoid and graphitic band (ratio D/G=1.03, Figure 3). After hydrazine reduction, the G-peak of RGO is gradually shifted to 1582 cm^{-1} and the D/G-ratio of the RGO increased slightly (ratio D/G=1.07). The shift of the G-peak and increase in the D/G ratio of RGO compared to graphene oxide are attributed to the restoration of sp_2 and, thus, more graphitic domains that are numerous but small in size.[3] Compared with GO, an increased D/G-ratio of 1.2 was observed for GO–PNI samples, indicating a largely disordered structure of the obtained samples, owing to the formation of covalent bonds between the GO and the PNI chains.[21] In other words, this result shows the formation of the sp_3 carbon after functionalization therefore, the data further confirm that the covalent modification of graphene sheets by PNI was successful.

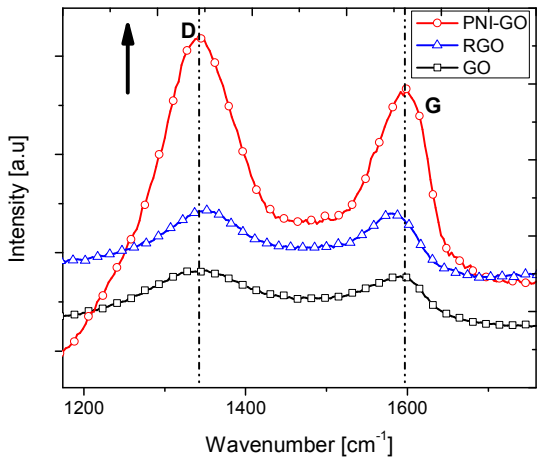

Figure 3: Raman data of GO, PNI-GO3 and PNI.

Thermal Analysis and Microscopy

The conclusion of PNI grafted to GO in the *in situ* polymerized samples is also supported by the results of the TGA experiments (Figure 4) performed on mostly dried samples. TGA graphs of the samples show that 0.17% GO (corresponding to 3% with respect to PNI) in a mostly dried sample led to a residue of 2.26% when heating to 800°C, while the initial sample should contain ca. 2.6% GO (and about 13% water based on T≈200°C). This corresponds to a residual of 90% with respect to the original GO content, although GO itself loses ca. 62% of its original weight at 800°C. Hence, the remaining mass must consist of PNI degradation products that do not detach from the GO surface. One might argue that this is an additive behaviour, but when estimating that the GO in PNI-GO3 should lead to a residue of 0.99% (38% of 2.6%) and that pure PNI leaves a residue of about 0.11%, the result of an expected residue of 1.1% is significantly below the experimentally observed value of 2.26%. A similar finding was reported by Zu and Han[41] for Pluronic and graphene sheets.

When comparing the findings for PNI-GO3 and the blend with an identical composition, it is clear that while the blend has slightly more residue than PNI, the residue is less than 20% of PNI-GO3. This shows that the *in situ* polymerization leads to significant permanent interactions (-> grafting) between GO and PNI, while the pure blending does not. Furthermore, it is also clear that the 0.44% of residue is significantly below the value of 0.90%, which is expected from the simple mixing rule by taking the initial H_2O content into account. Hence, it can be proposed that graphene attached to gaseous PNI residues more than doubles the weight loss of GO in the PNI-GO composites. Based on this argument, it is clear that the amount of arrested PNI degradation products on the GO sheets at 800°C is even higher than the 1.6%, one would expect based on the above arguments. Furthermore, it is also obvious that the degradation of PNI in PNI-GO3 is delayed by several degrees in comparison to PNI and the PNI+GO3 blend, again suggesting that simple blending does not lead to a strong attachment of PNI to GO.

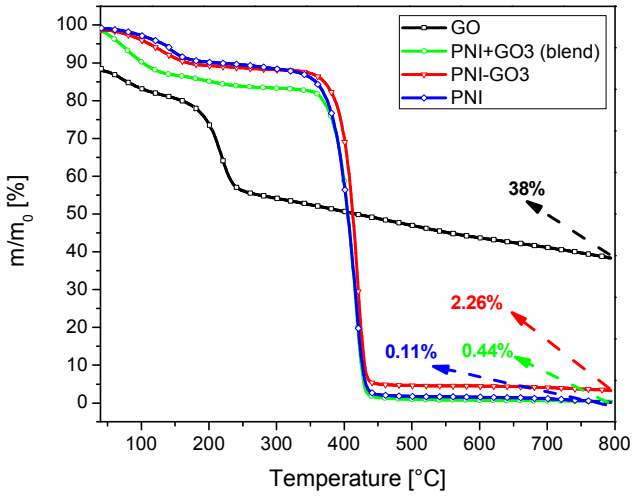

Figure 4. TGA curves of GO, PNI-GO3%PNI-GO3% blend and PNI.

The morphological structure of GO, PNI-GO3, and the blend were examined by TEM after washing and subsequently heating these samples to 800°C (Figure 5). It is clearly observed that the graphene oxide sheets have a smooth surface (Figure 5 a). When the samples are heated to 800°C, GO is thermally reduced and consequently, is almost transparent to electrons.[42] Thus, RGO is obtained and is slightly wrinkled, which is the consequence of the tendency of graphitic domains to stack (Figure 5b).[43, 44] The TEM image of the blend (PNI+GO3) sample before and after heating shows a few dark features (Figure 5c and d), which is the consequence of trace amounts of polymer residues due to the weak supramolecular interactions of PNI on the GO sheets. However, in Figure 5e and f, it is clearly observed that the PNI chains are grafted on the graphene oxide nanosheets by abundant spherical protuberances. Since the content of graphene is very low, a large amount of PNI molecules are immobilized on the same surface of one graphene oxide sheet. The surface modification of graphene oxide with PNI is not homogeneous, because PNI is initiated mainly via reactive groups and, thus, the active sites are not homogeneously distributed on the graphene oxide nanosheets. Similar phenomena have been reported for polymer brushes grafted onto substrates.[45] Figure 5g and h show the remains of the PNI-GO3 composite after heating the sample to 800°C. While the sheet structure of GO is retained, the sheets are crumbled and glued together by worm-like structures, which should be the remainder of the PNI grafted to the surface. Considering that the magnification of both images is approximately the same, it is cogent to assume that several GO sheets are stuck together. However, in the outer parts of the agglomerates, the sheet-like structure can still be seen to some degree. The finding is in agreement with Zu and Han as well as Kim *et al.*,[41, 46] who proved that polymers in the proximity of nanoparticles show a higher thermal stability.

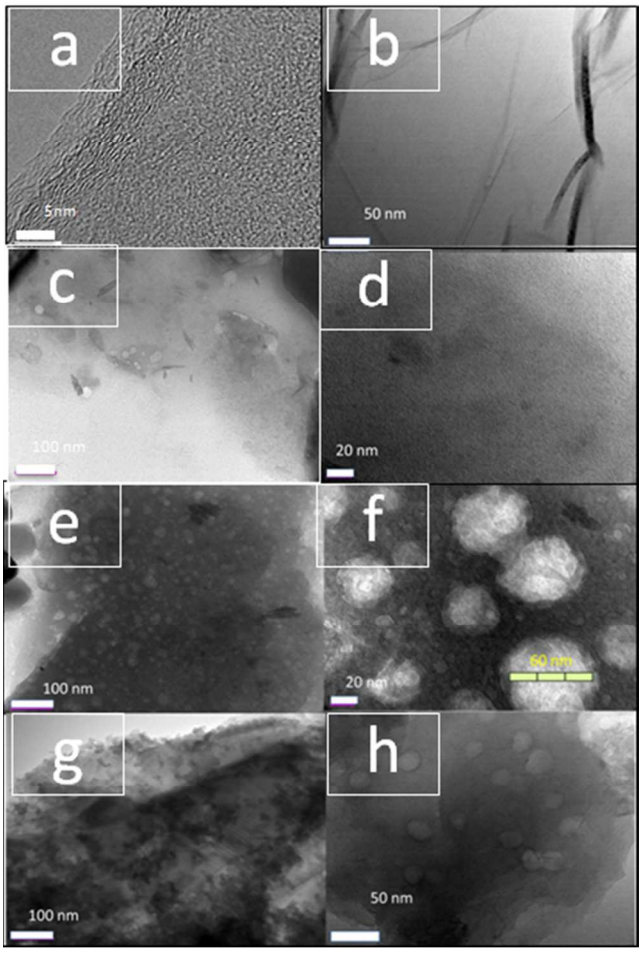

Figure 5. TEM image of (a) GO, (b) GO after 800°C, (c) PNI+GO3, (d) PNI+GO after 800°C (e, f) PNI-GO3 (g, h) and PNI-GO3 after 800°C

Rheology

Viscosity Function

Figure 6 shows the viscosity function, $\eta(\dot{\gamma})$, of a suspension of 0.5% GO in H_2O (i.e. a concentration ≈3 times the highest concentration in the composites) obtained after sonication to result in optimized dispersion. It appears a Newtonian plateau is only found for $\dot{\gamma}$>500 s^{-1}, while a quasi-yielding (not having the true yielding power law slope of -1 in $\eta(\dot{\gamma})$) is present for lower shear rates. This yielding is associated with the breakdown of H-bonding and mild re-orientation of GO at a high $\dot{\gamma}$. It is known that stable suspensions of GO can behave like colloids in H_2O thus avoiding agglomeration or restacking. The orientation anisotropy may produce a liquid crystal-like structure above a threshold of 0.5%, which can form a stable nematic liquid crystal in water.[47] The viscosity at high shear rates is around 3.5 mPas, which is somewhat higher than water (η=1 mPas) and clearly indicates that no significant interactions remain at high $\dot{\gamma}$ values.

The viscosity functions $\eta(\dot{\gamma})$ for PNI-GO0.25 (Figure 7a), PNI-GO2 (Figure 7b), and PNI-GO3 (Figure 7c) in principle resemble that of pure PNI, which was obtained previously.[48] However, at the lowest shear rates, the viscosity function clearly increases, which is typical for yielding. In regular polymers composites, this

kind of behaviour is usually only encountered at high filler concentrations.[49, 50] As the polymerization conditions are identical, the viscosity functions $\eta(\dot{\gamma})$ for GO concentrations between 0 and 2% for $\dot{\gamma}$>1 s^{-1} are very similar.

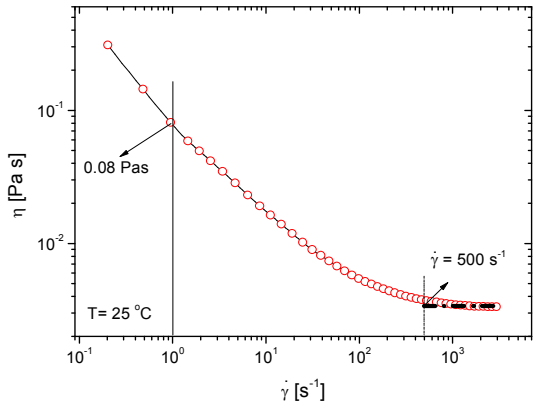

Figure 6. Viscosity function of a 0.5 wt.% GO-suspension

The viscosity functions for the other GO composites PNI-GO0.5 and PNI-GO1 are given in the Fig. SI4. The deviations in viscosity most likely stem from small differences of the molar mass, which originate from very small differences in the initiator and accelerator conditions and/or from the influence of the graphene oxide on the polymerization. Unfortunately, quantifying differences of the molar mass is not possible as performing *GPC* on samples with fillers is not feasible without seriously impairing the *GPC* device.

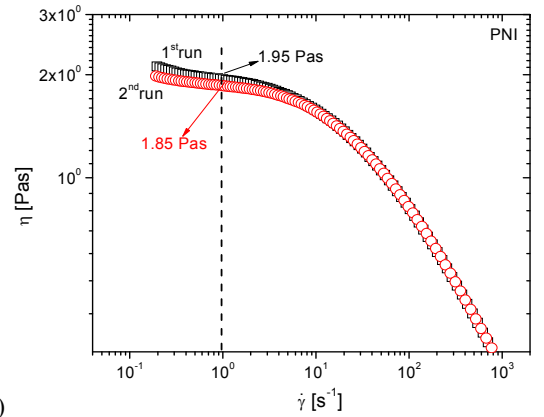

a)

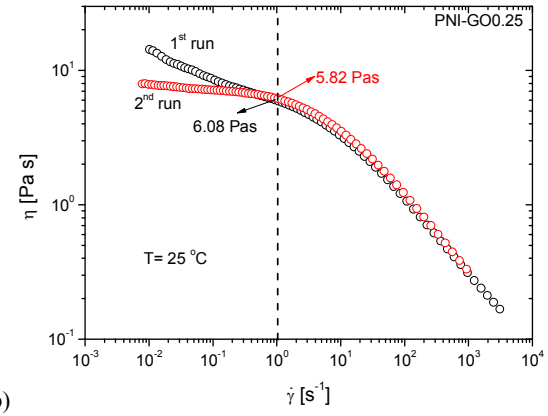

b)

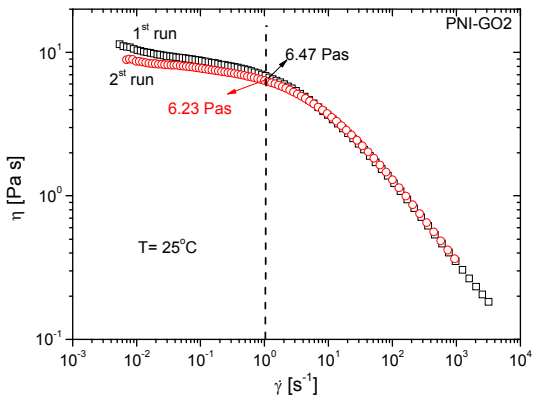

c)

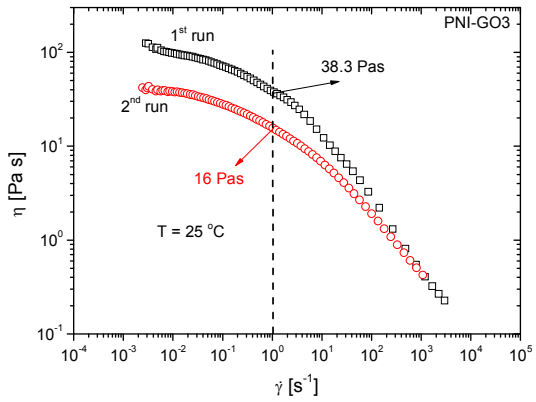

d)

Figure 7. viscosity functions at 25°C of a) PNI, b) PNI-GO0.25, c) PNI-GO2, d) PNI-GO3.

What can be said, however, is that the molar mass of all polymers is very high, as all samples clearly show signs of entanglement, although the concentration is below 6 wt.%. Based on Osaki *et al.'s* law for entanglements in solution,[51] it is concluded that the entanglement molar mass of the solution M_e^{sol} is $40\times M_e^{bulk}$ (for a dilution exponent α=1.3).[52] Although the exact entanglement molar mass M_e^{bulk} of PNI is unknown, literature suggests that it is around 15,000 g/mol.[53-56] Based on this value, it can be assumed that the molar mass $M_w\approx$3,000,000 g/mol of PNI is reasonable and that, furthermore, the PNI-GO-composites have comparable molar masses.

When repeating the test setup for $\eta(\dot{\gamma})$ with increasing shear rate immediately after reaching the maximum shear rate, the second run (red circles) shows distinctly lower viscosities for $\dot{\gamma}$<1-100 s^{-1} compared to the first run (black squares) for PNI-GO3, while for the samples with a lower concentration, a rather small difference between the first and second run is found at $\dot{\gamma}$ =1 s^{-1}.

The onset of the divergence increases with increasing GO content from $\dot{\gamma}\approx$0.5 s^{-1} at 0.25% to $\dot{\gamma}\approx$1000 s^{-1} at 3% suggesting that more intensive interactions exist, which is logical considering that the average distance between the GO sheets (with grafted PNI chains) scales with $c^{1/3}$. Hence, partial orientation leads to a complete loss of structure and thus, to a behaviour dominated by PNI alone, which is obvious as the disappearance of the increase of $\eta(\dot{\gamma})$ at low shear rates in the second run for GO-contents up to 2% and by a clear shape change of $\eta(\dot{\gamma})$ for PNI-GO3. An increase of the concentration delays the complete destructuring of the PNI-GO network, as interactions are possible due to the lower average distance between the GO sheets up to higher shear rates.

The ratio of $\eta(\dot{\gamma}=1\ s^{-1})_{run1}/\eta(\dot{\gamma}=1\ s^{-1})_{run2}$, indicated by the vertical lines in Figure 8, remains around unity for GO-contents up to 2%, while at $\dot{\gamma}=0.01\ s^{-1}$, a low GO-content leads to a significant reduction of viscosity ($\eta(\dot{\gamma}=0.01\ s^{-1})_{run1}/\eta(\dot{\gamma}=0.01\ s^{-1})_{run2}>1$), which is larger for PNI-GO0.25 than for PNI-GO2. The reduction of the difference can be interpreted to be due to the higher concentration which reduces the distance between the GO sheets and thus, makes reassembling a transient network structure faster. The only exception to these trends is PNI-GO3, which is not a liquid anymore and whose behaviour will be discussed in more detail later.

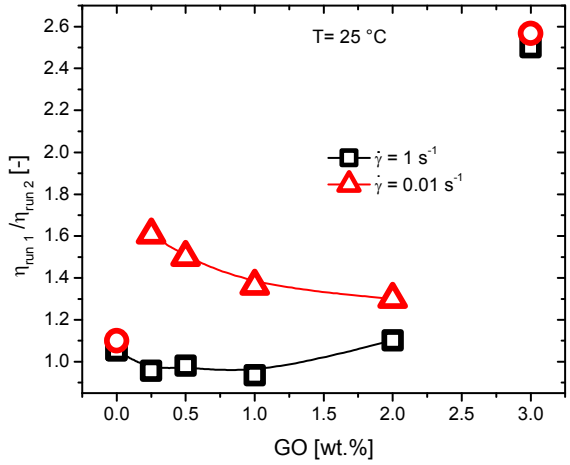

Figure 8. $\eta(\dot{\gamma}=1\ s^{-1})_{run1}/\eta(\dot{\gamma}=1\ s^{-1})_{run2}$ as a function of GO-concentration

Strain sweep

In dynamic mechanical experiments, the nonlinear behaviour was assessed by so called strain sweeps by taking measurements with increasing deformation, γ_0, at a constant frequency of $\omega=10\ s^{-1}$. In order to eliminate any existing structures in the sample, these experiments were carried out after the viscosity function test, which subjected the samples to intensive shear just before start of the experiment. Unlike classical polymer composites with significant amounts of µm-sized fillers, the GO composites have a linearity limit quite similar to that of unfilled polymer systems.[57, 58] When comparing the samples with 0.25% and 3% GO (Figure 9a/b), two clear differences are immediately obvious. Firstly, as the GO content increases, $\delta(\gamma_0<6\%)$ slightly decreases, which is expected as the introduction of fillers, in general, increases the elasticity. Secondly, the increase of GO content decreases the nonlinearity limit, γ_{NL}, defined by the onset of the increase of $\delta(\gamma_0)$. Due to the increase of the filler content, the surface area that PNI can interact with increases, which means that this trend is logical.

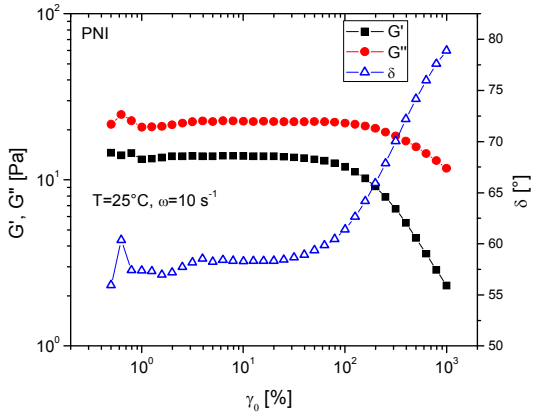

a)

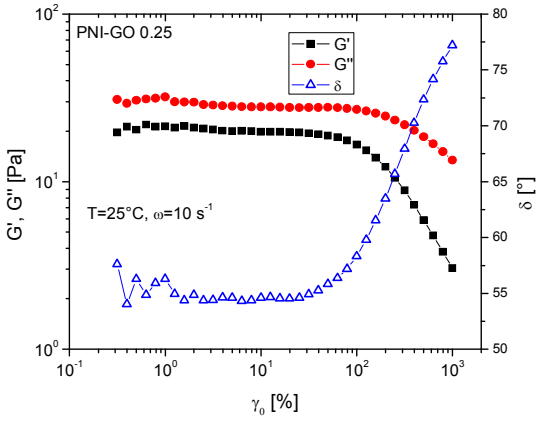

b)

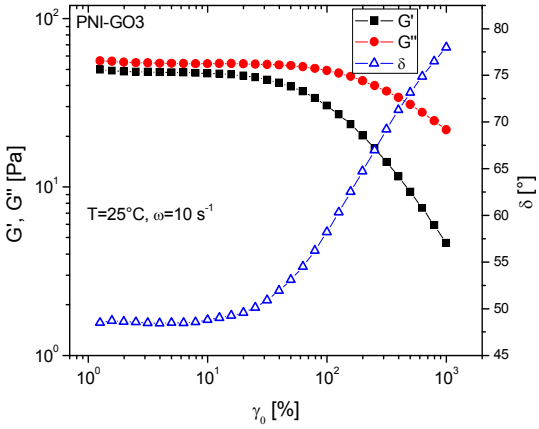

c)

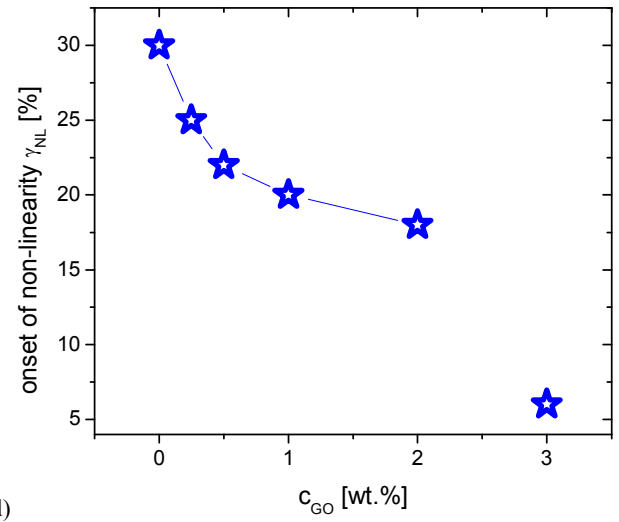

d)

Figure 9. strain sweeps of a) PNI, b) PNI-GO0.25, c) PNI-GO3 and d) onset of nonlinearity as a function of GO-concentration.

Figure 9d shows the linearity limit as a function of concentration, which demonstrates a clear decrease of γ_{NL}. However, while PNI-GO2 has a nonlinearity limit of 18%, PNI-GO3 shows γ_{NL}=6%, which clearly indicates that these samples have distinctly different structures, although their compositions are quite similar.

Creep Test

Figure 10 compares the creep and creep recovery behaviour of PNI and some of the different polymer solutions containing GO or RGO. The tests were performed at T=25°C or 5°C, depending on the viscosity. A deviation from the standard testing temperature of 25°C to 5°C was carried out if the sample viscosity was too low for performing the creep test at 25°C with reasonable accuracy. The shear stress, σ, was chosen to be 0.1 Pa or 1 Pa to determine the linearity of the measurements, which was found to be fulfilled for all samples.[59] Figure 10a shows that the "viscosity function" t/J(t) of PNI and PNI with 3% RGO reaches a Newtonian plateau quickly, which suggests that the zero shear-rate viscosity, η_0, was reached within the timeframe of the experiment. However, the samples with 2% and to an even larger degree 3% GO do not converge to a Newtonian plateau. Instead, they show an increasing viscosity, which is a typical effect related to a yield point, characteristic of polymers with significant amounts of fillers.[49, 50, 57] When comparing the samples with 2 and 3% GO, it becomes obvious that the onsets of the upturn occur around 1,500 s and 46 s, respectively. The power law slope at long times approaches 1, which is the maximum slope for systems with a yield point, indicating complete flow arrest. Hence, these samples have some solid-like characteristics, which is remarkable as the PNI solution is clearly a liquid and at the concentrations tested, 2% and 3% GO correspond to solids contents of 0.117 wt.% and 0.176 wt.%, respectively.

When comparing creep and creep recovery compliances, J(t) and $J_r(t_r)$ (Figure 10b and c), for the different samples, it becomes obvious that the recoverable compliance, $J_r(t_r>4{,}000\ s)$, of the samples is less than 1% of the creep compliances, J(t=4,000 s), for PNI and PNI-RGO3. In other words, in the terminal regime, the elasticity of these samples is negligibly small. For PNI-GO2, the elasticity is significantly higher, as can be seen in Figure 10b, demonstrating that $J_r(t_r>4{,}000\ s)$ is ca. 8% of J(t=4,000 s) and, thus, about 10 times more elastic than the samples mentioned above.

For PNI-GO3 (Figure 10c), J(t) and $J_r(t_r)$ are almost superimposed for $t=t_r<2{,}000$ s. Furthermore, the terminal value of J_r seems to approach the value of J(t=10,000 s). This indicates that indeed, the equation for the creep and creep recovery compliance

$$J(t) = J_0 + \psi(t) + \frac{t}{\eta_0} \quad (4)$$

$$J_r(t_r) = J_0 + \psi(t_r) \quad (5)$$

can be interpreted in such a way that $\eta_0 \to \infty$ and hence, $J(t) \approx J_r(t_r)$ for $t=t_r$. This type of behaviour is typical for viscoelastic solids, where complete recovery of the applied deformation is found with the same time dependence, i.e. $\psi(t) = \psi(t_r)$. Obviously, one would not expect that an almost ideal viscoelastic solid-like behaviour be obtained for a material with a solids content of only 0.176 wt.%, which shows the significant impact of the GO nanofillers in combination with the surface grafted chains, which collaboratively lead to this behaviour. What makes this behaviour even more surprising is the fact that after t=10,000 s, a total deformation of γ=420 % is observed, which is a very high value for a filler behaviour dominated material. Previously, such ideal rubber-like behaviour was observed for hydrogels in elongation but, unlike in this case, without a significant time dependence of the properties.[60] It is especially important to note that while 3% GO leads to a solid-like behaviour, the same amount of RGO has very little effect on the behaviour. While hydrazine reduction partially restores the aromaticity of graphene sheets, some surface defects undoubtedly remain. Thus, the reactivity of the graphene sheets will be changed and the distribution of grafting PNI chains will be affected due to such a decreased aromaticity. Another reason for this result may be due to the small amount of reactive oxygen containing moieties and smaller graphitic domains, as observed by Raman spectroscopy after reduction of the GO sheets. In other words, in the case of PNI-GO, the number of interactions with the carboxyl and hydroxyl decorated edges of the GO sheets is significantly higher, which leads to additional supramolecular interactions between $-COOH^-$ and $-NH^+$ responsible for forming a transient network.

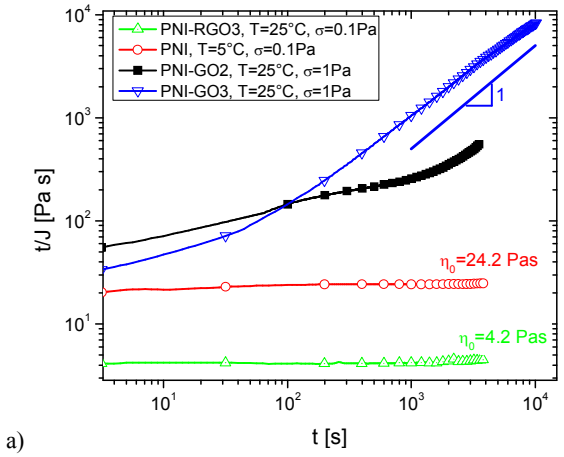

a)

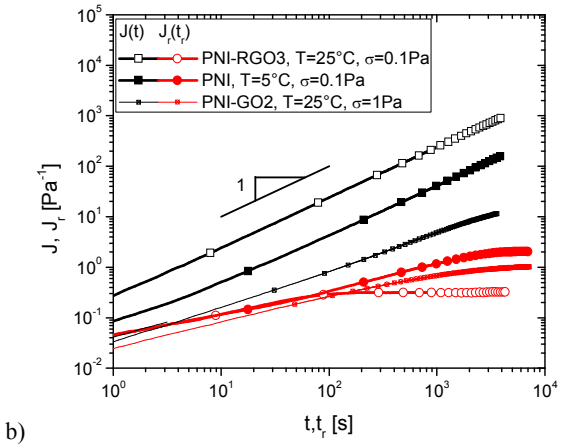

b)

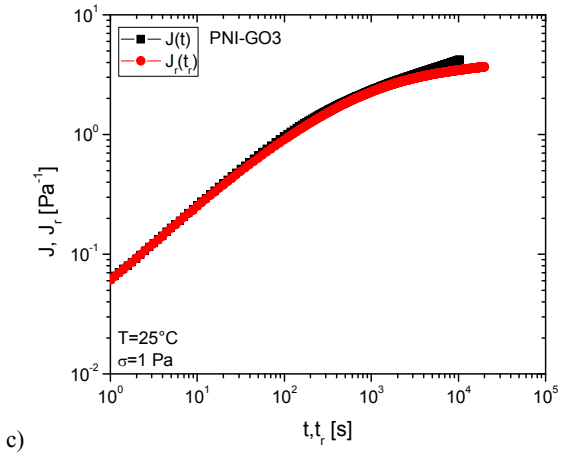

c)

Figure 10. creep data of PNI and GO and RGO-containing PNI-solutions. a) t/J, b) creep and creep recovery compliance of PNI, PNI-RGO3, and PNI-GO2, c) creep and creep recovery compliance of PNI-GO3

Conclusions

Discussion

In situ polymerized PNI-GO composites in aqueous solutions show a very interesting property profile. Based on the FTIR, TGA, TEM images and Raman spectroscopy, it can be concluded that surface-attached PNI chains exist in the centre of GO sheets predominantly containing residual C=C double bonds, with which PNI can react.[23, 24, 41] Meanwhile, the basal –COOH and –OH groups will supramolecularly interact with the PNI chains in aqueous media ((1), cf. Fig. 11) and thus, form a supramolecular network when having a sufficiently high concentration. Furthermore, clusters of GO sheets connected by PNI chains grafted to 2 or more sheets ((2),(4) Fig. 11) or connected by entangled loops of PNI chains ((3) Fig. 11) are permanently formed as well, although the low concentration of GO makes such clusters rather unlikely.

Rheological investigations are used to provide a sensitive insight into the mechanical properties, which will be evaluated in detail as probe to interaction patterns and molecular structure. The rheological data suggests that the supramolecular interaction basal GO plane with PNI forms a weak network structure, which can be easily destructured by high shear and takes some time to rebuild. For the composites with less than 2% GO, the recovery from destructuring is smaller as the GO content increases, which is due to the smaller distance that the PNI-chains has to travel to reattach. For a GO content of 3%, the behaviour is solid-like and, thus, a high shear leads to a loss of the network structure which, in turn, increases the difference between the first and second runs in the viscosity function. Likewise, the nonlinearity limit is also significantly lower for this sample, which suggests that the polymer chain dynamics are no longer the main determining factor but that the GO filler significantly influences the data as well. The creep data clearly shows that the roughly 400% deformation applied to the sample is recoverable, which suggests solid-like behaviour, albeit the very high deformation for a filled solid. It should be noted that PNI-GO2 also shows a significantly higher elasticity than the samples with lower GO contents, suggesting that the supramolecular network starts becoming stable enough for "solidifying" the sample. Considering all of this, it is safe to conclude that the rheological percolation threshold lies between GO contents of 2 and 3% (between total GO contents of 0.12 and 0.176%), which is comparable to values for polymer composites containing graphene oxide and other carbon-based fillers. CNT, for example, has a percolation threshold of 0.8-1.5%.[61] Although PNI-GO2 shows some characteristics of a viscoelastic solid, it clearly is a viscoelastic liquid. Simply blending GO and PNI solutions or using reduced GO instead of GO for the polymerization does not lead to the same results (Figure 11), although the PNI and filler concentrations are identical to PNI-GO3. These findings can be explained by the lack of permanent attachment of PNI to the GO surface for blends, which means that while it is possible that chains have an interaction with the basal GO planes, it does not have a large effect on the rheological behaviour as the chains are not anchored on the GO and thus, rather deplete the polymer solution and consequently result in a lower viscosity.

On the other hand, the use of RGO also leads to a sample, whose properties are mostly resembled by the pure PNI sample (Figure 11). This can be explained by the fact that it has been established that most of the basal –COOH and –OH groups disappear due to the reduction treatment (Figure SI2) and the aromaticity of graphene sheets are also partially restored,[3] which reduces the possibilities of interactions with PNI and H_2O and, furthermore, leads to a higher tendency of aggregation of RGO in aqueous dispersions. Hence, the structure of PNI-RGO3 is quite similar to

PNI-GO3, but with the decisive difference that the basal functionalities are mostly absent and that some aggregation has potentially taken place, which means that supramolecular interactions between RGO and PNI are almost absent. The comparisons of PNI-GO3 to the blended and RGO samples clearly show that for a solid sample, both surface-attached PNI and basal –COOH and –OH groups are necessary.

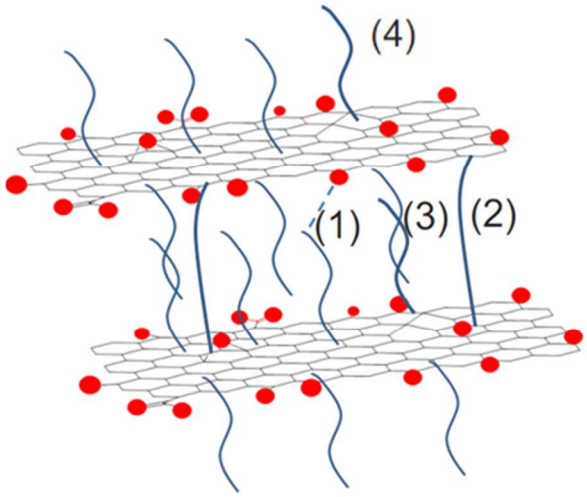

Interactions	PNI-GO	PNI-RGO	PNI+GO
1	✖		✖
2	✖	✖	
3	✖	✖	

Figure 11: schematic of the different interactions between the polymer chains and GO sheets.

Notes and references

[a] *College of Materials Science and Engineering, Shenzhen University, Shenzhen 518060, PR China and Chonbuk National University, School of Semiconductor and Chemical Engineering, Baekjero 567, Deokjin-gu, Jeonju, Jeonbuk, 561-756, Republic of Korea. Fax: +82 63 270 2306; Tel: +82 63 270 4039; E-mail: fjstadler@jbnu.ac.kr (general questions),*
[b] *Carbon Convergence Materials Research Center, Institute of Advanced Composite Materials, Korea Institute of -Science and Technology, San 101, Eunha-ri, Bongdong-eup, Wanju-gu, Jeonbuk, 565-905, Republic of Korea*
[c] *Department of Chemical Engineering, NED University of Engineering & Technology, University Road, Karachi-75270, Pakistan.*
[d] *Islamic Azad University, Omidiyeh Branch, Department of Polymer, 63731-93719, Omidiyeh, Iran. E-mail: mvatankhahs@yahoo.com*
† Electronic Supplementary Information (ESI) available: TEM-images of GO, FTIR of GO & RGO, Raman Spectroscopy of GO & RGO, and some more experimental details. See DOI: 10.1039/b000000x/

The authors acknowledge financial aid from the National Research Foundation of Korea (110100713) and "Human Resource Development (Advanced track for Si-based solar cell materials and devices, project number: 20124030200080)" of the Korea Institute of Energy Technology Evaluation and Planning (KETEP) grant funded by the Korea government Ministry of Knowledge Economy. The authors would also like to thank the staff of the CBNU central lab especially Ms. Song-I Kim.

1. D. R. Dreyer, S. Park, C. W. Bielawski and R. S. Ruoff, *Chemical Society reviews*, 2010, **39**, 228-240.
2. A. Lerf, H. Y. He, M. Forster and J. Klinowski, *Journal of Physical Chemistry B*, 1998, **102**, 4477-4482.
3. S. Stankovich, D. A. Dikin, R. D. Piner, K. A. Kohlhaas, A. Kleinhammes, Y. Jia, Y. Wu, S. T. Nguyen and R. S. Ruoff, *Carbon*, 2007, **45**, 1558-1565.
4. F. Kim, L. J. Cote and J. Huang, *Adv Mater*, 2010, **22**, 1954-1958.
5. J. Luo, L. J. Cote, V. C. Tung, A. T. Tan, P. E. Goins, J. Wu and J. Huang, *J Am Chem Soc*, 2010, **132**, 17667-17669.
6. J. Kim, L. J. Cote, F. Kim and J. Huang, *J Am Chem Soc*, 2010, **132**, 260-267.
7. J. Kim, L. J. Cote, F. Kim, W. Yuan, K. R. Shull and J. Huang, *J Am Chem Soc*, 2010, **132**, 8180-8186.
8. O. C. Compton and S. T. Nguyen, *Small*, 2010, **6**, 711-723.
9. L. Q. Xu, W. J. Yang, K. G. Neoh, E. T. Kang and G. D. Fu, *Macromolecules*, 2010, **43**, 8336-8339.
10. J. I. Paredes, S. Villar-Rodil, A. Martinez-Alonso and J. M. D. Tascon, *Langmuir : the ACS journal of surfaces and colloids*, 2008, **24**, 10560-10564.
11. M. Fang, K. G. Wang, H. B. Lu, Y. L. Yang and S. Nutt, *Journal of Materials Chemistry*, 2010, **20**, 1982-1992.
12. C. S. Shan, H. F. Yang, D. X. Han, Q. X. Zhang, A. Ivaska and L. Niu, *Langmuir : the ACS journal of surfaces and colloids*, 2009, **25**, 12030-12033.
13. H. J. Salavagione and G. Martinez, *Macromolecules*, 2011, **44**, 2685-2692.
14. I. W. Hamley, *Introduction to Soft Matter: Synthetic and Biological Self-Assembling Materials*, John Wiley & Sons Ltd, Chichester, UK 2007.
15. T. A. Witten and P. A. Pincus, *Structured Fluids: Polymers, Colloids, Surfactants*, Oxford University Press, New York, 2004.
16. S. Nayak and L. A. Lyon, *Angew Chem Int Edit*, 2005, **44**, 7686-7708.
17. E. Kokkoli, A. Mardilovich, A. Wedekind, E. L. Rexeisen, A. Garg and J. A. Craig, *Soft Matter*, 2006, **2**, 1015-1024.
18. V. Vitelli and M. van Hecke, *Nature*, 2011, **480**, 325-326.
19. S. Hashmi, A. GhavamiNejad, F. O. Obiweluozor, M. Vatankhah-Varnoosfaderani and F. J. Stadler, *Macromolecules*, 2012, **45**, 9804-9815.
20. B. J. Hong, Z. An, O. C. Compton and S. T. Nguyen, *Small*, 2012, **8**, 2469-2476.
21. S. M. Zhu, J. B. Li, Y. H. Chen, Z. X. Chen, C. X. Chen, Y. Li, Z. W. Cui and D. Zhang, *J Nanopart Res*, 2012, **14**.
22. Y. F. Yang, X. H. Song, L. Yuan, M. Li, J. C. Liu, R. Q. Ji and H. Y. Zhao, *J Polym Sci Pol Chem*, 2012, **50**, 329-337.
23. J. J. Qi, W. P. Lv, G. L. Zhang, F. B. Zhang and X. B. Fan, *Polymer Chemistry*, 2012, **3**, 621-624.
24. J. Dong, J. Weng and L. Z. Dai, *Carbon*, 2013, **52**, 326-336.
25. H. Muenstedt, N. Katsikis and J. Kaschta, *Macromolecules*, 2008, **41**, 9777-9783.
26. J. T. Robinson, S. M. Tabakman, Y. Y. Liang, H. L. Wang, H. S. Casalongue, D. Vinh and H. J. Dai, *J Am Chem Soc*, 2011, **133**, 6825-6831.
27. Y. Z. Pan, H. Q. Bao, N. G. Sahoo, T. F. Wu and L. Li, *Advanced Functional Materials*, 2011, **21**, 2754-2763.
28. D. Depan, P. K. C. V. Surya, B. Girase and R. D. K. Misra, *Acta Biomater*, 2011, **7**, 2163-2175.
29. J. F. Shen, B. Yan, M. Shi, H. W. Ma, N. Li and M. X. Ye, *Journal of colloid and interface science*, 2011, **356**, 543-549.
30. R. D. Priestley, C. J. Ellison, L. J. Broadbelt and J. M. Torkelson, *Science*, 2005, **309**, 456-459.
31. A. R. Payne, *Journal of Applied Polymer Science*, 1962, **6**, 57-63.
32. P. Starck, W. K. J. Mosse, N. J. Nicholas, M. Spiniello, J. Tyrrell, A. Nelson, G. G. Qiao and W. A. Ducker, *Langmuir : the ACS journal of surfaces and colloids*, 2007, **23**, 7587-7593.
33. S. Abbasi, P. J. Carreau, A. Derdouri and M. Moan, *Rheologica Acta*, 2009, **48**, 943-959.
34. S. Hashmi, F. Obiweluozor, A. GhavamiNejad, M. Vatankhah-Varnoosfaderani and F. J. Stadler, *Korea-Australia Rheology Journal*, 2012, **24**, 191-198.

35. S. Hashmi, M. Vatankhah-Varnoosfaderani, A. GhavamiNejad, L. Mespouille, F. O. Obiweluozor and F. J. Stadler, *Macromolecules*, 2013, **submitted**.
36. J. F. Shen, B. Yan, T. Li, Y. Long, N. Li and M. X. Ye, *Compos Part a-Appl S*, 2012, **43**, 1476-1481.
37. J. Q. Liu, W. R. Yang, L. Tao, D. Li, C. Boyer and T. P. Davis, *J Polym Sci Pol Chem*, 2010, **48**, 425-433.
38. S. G. Miller, J. L. Bauer, M. J. Maryanski, P. J. Heimann, J. P. Barlow, J. M. Gosau and R. E. Allred, *Composites Science and Technology*, 2010, **70**, 1120-1125.
39. B. Adhikari, A. Biswas and A. Banerjee, *Langmuir : the ACS journal of surfaces and colloids*, 2012, **28**, 1460-1469.
40. L. Wei, F. Wu, D. Shi, C. Hu, X. Li, W. Yuan, J. Wang, J. Zhao, H. Geng, H. Wei, Y. Wang, N. Hu and Y. Zhang, *Scientific reports*, 2013, **3**, 2636.
41. S. Z. Zu and B. H. Han, *J Phys Chem C*, 2009, **113**, 13651-13657.
42. D. Joung, L. Zhai and S. I. Khondaker, *Phys Rev B*, 2011, **83**.
43. Y. F. Dong, S. Li, H. M. Xu, M. Y. Yan, X. M. Xu, X. C. Tian, Q. Liu and L. Q. Mai, *Phys Chem Chem Phys*, 2013, **15**, 17165-17170.
44. Y. Y. Feng, H. P. Liu, W. Luo, E. Z. Liu, N. Q. Zhao, K. Yoshino and W. Feng, *Sci Rep-Uk*, 2013, **3**.
45. L. L. Ren, S. Huang, C. Zhang, R. Y. Wang, W. W. Tjiu and T. X. Liu, *J Nanopart Res*, 2012, **14**.
46. Y. Kim, V. R. Babu, D. T. Thangadurai, K. S. V. K. Rao, H. Cha, C. Kim, W. Joo and Y. I. Lee, *B Korean Chem Soc*, 2011, **32**, 553-558.
47. Z. Xu and C. Gao, *Nat Commun*, 2011, **2**.
48. A. G. Saud Hashmi, Mohammad Vatankhah-Varnoosfaderani, Francis O. Obiweluozora, Florian J. Stadlera*, *Rheologica Acta*, 2014.
49. M. Schmidt and H. Münstedt, *Rheologica Acta*, 2002, **41**, 193-204.
50. M. Schmidt and H. Münstedt, *Rheologica Acta*, 2002, **41**, 205-210.
51. K. Osaki, Y. Nishimura and M. Kurata, *Macromolecules*, 1985, **18**, 1153-1157.
52. F. J. Stadler, M. Rajan, U. S. Agarwal, C.-Y. Liu, K. E. George, P. J. Lemstra and C. Bailly, *Rheologica Acta*, 2011, **50**, 491-501.
53. N. Seetapan, K. Mai-ngam, N. Plucktaveesak and A. Sirivat, *Rheologica Acta*, 2005, **45**, 1011-1018.
54. H. Chen, W. Li, H. Zhao, J. Gao and Q. Zhang, *Journal of colloid and interface science*, 2006, **298**, 991-995.
55. Y. Tsuboi, T. Tada, T. Shoji and N. Kitamura, *Macromolecular Chemistry and Physics*, 2012, **213**, 1879-1884.
56. J. Ye, J. Xu, J. Hu, X. Wang, G. Zhang, S. Liu and C. Wu, *Macromolecules*, 2008, **41**, 4416-4422.
57. J. D. Ferry, *Viscoelastic Properties of Polymers*, John Wiley and Sons, New York, 1980.
58. C. W. Macosko, *Rheology: Principles, Measurements and Applications*, Wiley/VCH, Poughkeepsie, NY 1994.
59. F. Wolff, J. A. Resch, J. Kaschta and H. Münstedt, *Rheologica Acta*, 2010, **49**, 95-103.
60. F. J. Stadler, T. Friedrich, K. Kraus, B. Tieke and C. Bailly, *Rheologica Acta*, 2013, **52**, 413-423.
61. P. Pötschke, T. D. Fornes and D. R. Paul, *Polymer*, 2002, **43**, 3247-3255.